Localized Ti^{III} mediated dissociative electron transfer for carbon halogen bond activation on TiO_2

Qian Zhu [a,b], Yuanyuan Wang [a,b], Hongna Zhang [a,b], Ran Duan [a,b], Chuncheng Chen [a,b], Wenjing Song [a,b,*], Jincai Zhao [a,b]

[a] Key Laboratory of Photochemistry, CAS Research/Education Center for Excellence in Molecular Sciences, Institute of Chemistry, Chinese Academy of Sciences, Beijing 100190, PR China
[b] University of Chinese Academy of Sciences, Beijing 100049, PR China

ARTICLE INFO

ABSTRACT

The reductive activation of the carbon halogen (C-X) bond is a key step in the transformation of organic halides via bond dissociation. Monochloroacetic acid (MCA), a typical recalcitrant aliphatic halide, was previously shown to be reduced by hydrated electrons (e_{aq}), requiring 254 nm irradiation. Here, we demonstrate the efficient hydrogenation of MCA to acetic acid (HOAc) with high selectivity using TiO_2 electrons accumulated under the bandgap (3.2 eV) excitation in the presence of methanol as a hole scavenger. The reaction occurs via a single electron transfer in concert with C-Cl cleavage (concerted dissociative electron transfer, DET) to give $^{\bullet}CH_2COOH$, which is then subjected to the subsequent $1e^-/1H^+$ process to give HOAc. The in situ visible and infrared spectroscopic characterizations reveal the critical role of localized Ti^{III} states in C-Cl activation, whereas conduction band or shallow trapped electrons are not active in this process. The photocatalytic reduction rate slowed down with an increase in the intervening carbon atoms (monohalogenated propionic and butyric acids) between TiO_2 surface and the C-X bond, which is attributed to the decrease in the electron transfer driving force.

© 2017 Elsevier B.V. All rights reserved.

1. Introduction

The reductive activation of the carbon halogen bond is one of the most important processes in the elimination of halogenated contaminants [1]. Various systems have been developed for their reductive conversion, such as zero-valent iron (ZVI) and Pd/Fe nanoparticles [2–4], supported metal catalysts (ZrO_2/Pd in the presence of H_2) and metal electrodes (e.g., Ag/Cu/Pd-on carbon or Cu on graphene) [5–9], and semiconductor-based photo(electro)catalysis [10,11]. In general, reductive conversion rates slow down as decrease in the number of geminal halogen atoms, and less halogenated compounds are more resistant. For chloroacetic acids, the reduction of tri- and di- chloroacetic acid (TCA, DCA) occurs on ZVI, but almost no conversion is found for MCA [2]; in addition, the successful photoelectrochemical reduction of TCA and DCA can be realized on silicon carbide photocathodes, while MCA is not [11]. These findings can be understood by a more negative reduction potential of MCA (-0.6 V for TCA, −1.31 V for DCA and −1.43 V for

MCA; all potentials are against the standard hydrogen electrode, SHE) [11]. The reduction potential is a marker for bond dissociation energy and the electron transfer thermodynamic driving force, which dictates the reaction kinetics. Indeed, MCA reduction poses a great challenge, and most abiotic methods fail. Palladium-modified materials can reduce MCA by surface hydrogen species but the employment of noble-metal limits the application. Hydrated electron (e_{aq}) with a reduction potential of −2.9 V vs. SHE is capable of triggering MCA conversion to acetic acid (HOAc), succinic acid, and other non-chlorinated products [12]. However the production of e_{aq} necessitates a high energy input, requiring deep-UV (254 nm) irradiation [12], radiolysis [13], or a delicate design for a tandem two-photon process incorporating energy and electron transfer [14]. The reductive detoxification of MCA catalyzed by earth abundant materials and/or driven by lower energy photons would be highly favored.

Titanium dioxide is a prototype photocatalyst that achieves redox conversion via the valence band hole and conduction band electrons. The reduction of versatile organic functional groups, including carbonyl, nitro, and epoxy groups, was observed on TiO_2 under electrochemical charging or photocatalytic conditions in the presence of a hole scavenger [15–21]. The broad distribution of the density of states, corresponding to different chemical structures (free conduction band electrons, shallow trapped electron or local-

---

ized Ti^{3+} states in the bandgap), results in the potential-dependent electron transfer kinetics [16,18]. Molinari A. et al. demonstrated that the reduction of the nitro group begins at 70 mV below the conduction band; however, the hydrogenation of an aldehyde carbonyl occurs only when the TiO_2 Fermi level approaches the conduction band edge [18]. Notably, TiO_2 catalyzes the deoxygenation of epoxides (which have more negative one electron reduction potentials than that of its conduction band) via a concerted two-electron transfer from the surface Ti^{3+} sites [19,20]. The hydrogenation of organic halides, including decabromodiphenyl ether (BDE 209), hexabromobenzene, CCl_4 and TCA, mediated by TiO_2 has also been demonstrated by several groups, including ours [22–25]. Recently we revealed a proton addition induced hydrogenation of non-adsorbable aromatic halides by solvent kinetic isotope study. In contrast, the rate-determining step of photocatalytic TCA reduction does not involve proton transfer [22].

In this study, we further explore the reductive activity of the TiO_2 electron towards a series of halogenated aliphatic acids (monochloro-/monobromo-, acetic, propionic, and butyric acids) and the electron-proton transfer mechanism. Notably, MCA converts to HOAc and Cl^- with high selectivity under photocatalytic condition with UV irradiation above 360 nm, or by electrons pre-accumulated on TiO_2. According to the open circuit potential (OCP) decay profile and in situ spectroscopic (UV-vis and mid-infrared region, MIR) measurements, the localized Ti^{III} states are active for MCA reduction, whereas the free conduction band and shallow trapped electrons have significantly less contribution. The correlation of the reaction kinetics with the reduction potential of the investigated model compounds, is consistent with an electron transfer-controlled process. And the initial electron transfer occurs concomitantly with C-X cleavage (concerted DET). The distinct chemical nature of TiO_2 electrons and the different activities observed for interfacial reductive transformations reveal the potential of metal oxide semiconductor based photocatalysis for decontamination of waste water with organic halides.

2. Experimental

2.1. Materials

TiO_2 (P25) was obtained from Evonik (Degussa) Company and was irradiated in aqueous solution under UV light for 24 h prior to use. The TiO_2 was then subjected to centrifugation, filtration, and calcination at 450 °C for 3 h to remove the adsorbed organic species [22]. Anatase (15 nm) was obtained from Alfa Aesar Co., and rutile (<100 nm) was purchased from Sigma-Aldrich Co. Pt-TiO_2 (0.5 wt%) was prepared by photocatalytic reduction method [19]. Briefly, 150 mL aqueous suspension containing 1 g TiO_2, 10 mL CH_3OH and 1.325 mL $H_2PtCl_6 \cdot 6H_2O$ aqueous solution (0.02 M) was deaerated and irradiated with 300 W Xe lamp for 2 h under vigorous stirring. MCA and 4-bromobutyric acid were obtained from Alfa Aesar Co. 3-Chloropropionic acid, 4-chlorobutyric acid and 3-bromopropionic acid were purchased from Sigma-Aldrich Co. Bromoacetic acid, ethyl chloroacetate, ethyl bromoacetate, ethyl 3-chloropropionate, ethyl 3-bromopropionate, 1,10-phenanthroline, N-methylpyrrole and tetrabutylammonium tetrafluoroborate were purchased from J&K Chemicals Co. Ethyl 4-chlorobutyrate and ethyl 4-bromobutyrate were obtained from TCI (Shanghai) Development Co., Ltd. Methanol and acetonitrile were of HPLC grade (Dikma Technologie) and were used without further purification.

2.2. Photocatalytic reactions

In a typical photocatalytic experiment, TiO_2 (0.5 g/L) was added to a 20 mL methanol solution containing MCA or other halocar-

boxylic acids (1 mM). The suspension was sealed in a Pyrex vessel and purged with Ar for 30 min to remove O_2 before irradiation. A 300 W Xe lamp (Beijing Aulight Technology Co.) was used as the light source, and a cutoff filter ($\lambda > 360$ nm) was used to prevent the direct photolysis of the substrates. The reaction temperature was maintained at 303 K via a constant temperature circulator (Beijing YKKY Technology Co., Ltd). A portion of the suspension (1 mL) was collected at given time intervals and centrifuged. The supernatant of each sample was analyzed by Ionic Chromatography (IC) using DX-900 ion chromatography with an IonPac AS19 column (Thermo). The eluent was a 5 mM KOH solution, and the suppressor current was 20 mA for monochloro carboxylic acids. For brominated carboxylic acids, the eluent was a 7 mM KOH solution and the current was 28 mA. The elute flow rate was 1 mL/min. The photocatalytic degradation of MCA by Pt-TiO_2 was carried out under the same experimental conditions as that of TiO_2. In addition, H_2 was quantified at the same time by gas chromatography (GC) equipped with a thermal conductivity detector (TCD) detector.

The pre-irradiation experiment was conducted in the same Pyrex vessel with a TiO_2 (2 g/L) suspension in methanol solution but in the absence of MCA. After purged with Ar for 30 min, the suspension was irradiated for 3 h. The TiO_2 suspension changed from white to blue as electrons accumulated on TiO_2 during irradiation [16]. The electron concentration was measured using the Fe^{3+}-1,10-phenanthroline spectrometric titration method [26] (Supplemental contents).

2.3. Measurements and characterizations

The morphologies of the TiO_2 (P25) before and after reaction were characterized by a SU8010 scanning electron microscope (SEM). Transmission electron microscope (TEM) and high-resolution transmission electron microscope (HRTEM) images of TiO_2 were taken on a JEM-2011F electron microscope.

Open circuit potential (OCP) experiment was conducted in a three-electrode system. The working electrode was a TiO_2/FTO (F-doped tin oxide) film electrode prepared as previously reported [18], the counter electrode was a Pt wire, and the reference electrode was Ag/AgCl. The open circuit potential was measured on a CHI760D electrochemical workstation. A Xe lamp was used as the light source. The experiment was performed in Ar saturated CH_3OH solution using n-Bu_4NClO_4 (0.1 M) as the supporting electrolyte. MCA (1 mM) was added to the electrolyte solution as necessary. The open circuit potential decay post UV illumination was used to calculate the electron lifetime using Eq. (1) [27], where τ is the lifetime, k_B is Boltzmann's constant, T is the temperature in K, e is the charge of a single electron, and V_{oc} is the open circuit potential at time t.

$$\tau = \frac{k_B T}{e} \left(\frac{dV_{OC}}{dt} \right)^{-1} \tag{1}$$

Cyclic voltammetry (CV) of halogenated carboxylic ethyl esters were obtained on the same CHI760D electrochemical workstation with the three-electrode system in which the working electrode was glassy carbon. All electrochemical measurements were performed in Ar-saturated CH_3CN solution with n-Bu_4NBF_4 (0.1 M) as the supporting electrolyte. Halogenated compound concentrations were 1 mM. Scan rate was 50 mV s^{-1}.

UV-vis reflectance spectra of the irradiated suspensions were collected on a fiber-optical spectrometer (Ocean Optics), equipped with a HL-2000-FHAS light source and a USB2000+ detector. TiO_2 particles (150 mg) were added to a 3 mL Ar-purged methanol solution or MCA-containing methanol solution (5 mM); this mixture was sealed in a quartz cuvette and stirred during the experiment to prevent subsidence. A 3 W 365 nm LED was used as the light source.
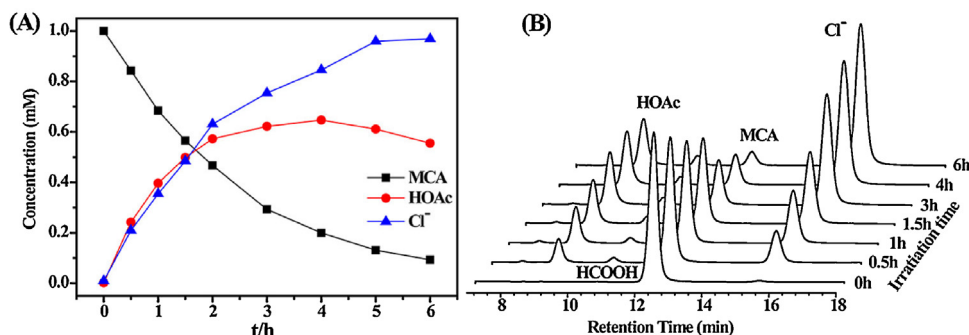
Fig. 1. (A) Change in the concentrations of MCA, HOAc and Cl$^-$ under photocatalytic condition in the presence of 0.5 g/L TiO$_2$ under irradiation provided by a Xe lamp with a 360 nm cutoff filter (the light intensity was 120 mW cm^{-2}) at 303 K. (B) IC chromatograms of the supernatant after centrifugation at the indicated time (the peak at 10.6 min is HCOOH generated from methanol oxidation).
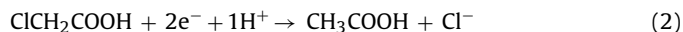
The ATR-MIR measurements were performed on a Nicolet 6700 FT-IR instrument with a mercury cadmium telluride (MCT) detector. IR spectra ranging from 4000 to 1000 cm^{-1} were recorded by averaging 32 scans with a resolution of 4 cm^{-1}. The TiO$_2$ film was coated on a ZnSe crystal. Methanol or a substrate-containing methanol solution (1.5 mL) was dripped onto the film surface and then purged with Ar for 5 min at a flow rate of 20 mL/min. After adsorption equilibrium was achieved, the background spectrum was collected. Then a 3 W 365 nm LED was used as light source.

3. Results and discussion

The photocatalytic reaction was performed in an Ar-saturated 1 mM MCA methanol solution in the presence of P25 TiO$_2$ (0.5 g/L) under an irradiation above 360 nm. Methanol was used as the solvent and hole scavenger. Under this condition, electrons are accumulated on TiO$_2$ and is available for reaction. The suspension was stirred in the dark for 30 min before irradiation. There was no significant change in the concentration of MCA in the dark, as quantified by ionic chromatography (IC). Fig. 1A shows the MCA concentration-time profile under irradiation, revealing pseudo-first order kinetics with a k$_{obs}$ of 1.1×10^{-4} s^{-1} for MCA decomposition, which is accompanied by the generation of Cl$^-$ and HOAc (Fig. 1B). The rate constant of Cl$^-$ production agrees with that of MCA decomposition (k$_{obs}$ = 1.3×10^{-4} s^{-1}). The conversion to HOAc is quantitative in the first 1.5 h. The decrease in HOAc concentration afterwards could be caused by the acid-catalyzed esterification of acetic acid with methanol (Fig. S1) as the concentration of proton (generated by methanol oxidation, CH$_3$OH → CH$_2$O + 2H$^+$) continues to increase during photocatalytic reaction. No other reduction products of MCA degradation (e.g., succinate) were observed under photocatalytic condition (Fig. 1B). The TiO$_2$ catalyst remained intact and no surface corrosion was observed after photocatalytic reduction as evidenced by SEM and TEM (Fig. S2). Photoreduction of MCA to HOAc and Cl$^-$ was also achieved using rutile or anatase as the catalyst (Fig. S3).

Under our experimental conditions, methanol oxidation produces strongly reducing $^\bullet$CH$_2$OH intermediates that may directly reduce MCA [23]. To determine the active reducing species, electrons were pre-stored before addition of MCA, giving the typical bluish color, which is stable for hours in the absence of an electron acceptor [16]. The addition of Ar-purged MCA stock solution (final concentration 1 mM) to the pre-irradiated TiO$_2$ suspension resulted in the consumption of all the stored electrons, as evidenced by the color change from blue to white. Concomitantly, the generation of HOAc and Cl$^-$ from MCA was confirmed by IC. The reacted electrons were quantified using the Fe^{3+}-1, 10-phenanthroline spectrometric titration method. A MCA to electron concentration ratio of 1: 2 was obtained (Table S1, entry 1), which was consistent with an overall

2e$^-$/1H$^+$ process for the hydrogenation of C-Cl (Eq. (2)). The role of TiO$_2$(e$^-$) was also confirmed by the 5-fold lower photostationary electron concentration in the presence of MCA (Fig. 2A). These results verify that TiO$_2$(e$^-$) is responsible for the hydrogenation of MCA. Further evidence for the interfacial electron transfer process was revealed by the decrease in the electron lifetime (extracted from the open circuit potential-time profile post irradiation) with added MCA (Fig. 2B) [28]. Intriguingly, electrons at the intermediate energy are most active, as estimated from changes in the electron lifetime at different potentials (Fig. 2B, right panel). Details of the different activities of TiO$_2$(e$^-$) towards MCA reduction are discussed in more detail below.

$$ClCH_2COOH + 2e^- + 1H^+ \rightarrow CH_3COOH + Cl^- \tag{2}$$

In our open circuit potential measurement, the change in electron lifetime suggests the potential determined activities of the TiO$_2$ electrons. The higher V$_{oc}$ region corresponds to free electrons in the conduction band/shallow trapped electrons (0.1 − 0.2 eV below conduction band), while in the lower V$_{oc}$ region, bulk or surface localized electronic states are occupied [29]. The electron lifetime shown in Fig. 2B demonstrates a higher activity of states within the intermediate potential regime, which suggests that electron transfer to MCA is dominated by localized electronic states within the band gap.

To further identify the chemical nature of the active states, in situ UV–vis and MIR spectroscopic measurements were performed. The characteristic blue color of reduced TiO$_2$ (a broad absorption from 480 nm that extends to ~2000 nm) has been assigned to the localized Ti^{III} states within the bandgap (trap states), whereas the free conduction band electrons and/or a shallow trapped electrons that are in thermal equilibrium with the conduction band electrons give the broad IR absorption feature whose intensity increases monotonically with the wavenumber from 1000 to 3000 cm^{-1} [30–32]. The UV–vis spectra of the reaction suspension were monitored under 365 nm irradiation provided by a 3 W LED. As shown in Fig. 3A–C, in the presence of 5 mM MCA, the broad absorption above 480 nm decreased dramatically and the steady state absorption at 700 nm were only 10% of those without MCA, verifying that electron transfer from the localized Ti^{III} state to MCA. The activity of Ti^{III} was also supported by the electron spin resonance (ESR) measurements, where the characteristic signal of Ti^{III} with a g tensor of 1.957 depleted upon introduction of MCA (Fig. S4) [30].

The role of the free conduction band and/or shallow trapped electrons were investigated using in situ attenuated total reflection infrared (ATR-IR) spectroscopy. In this test, a TiO$_2$ thin film (2–3 μm) was coated on a ZnSe crystal, and all the spectra were taken with reference to the sample spectra before irradiation. The broad MIR absorption was not significantly changed in the presence
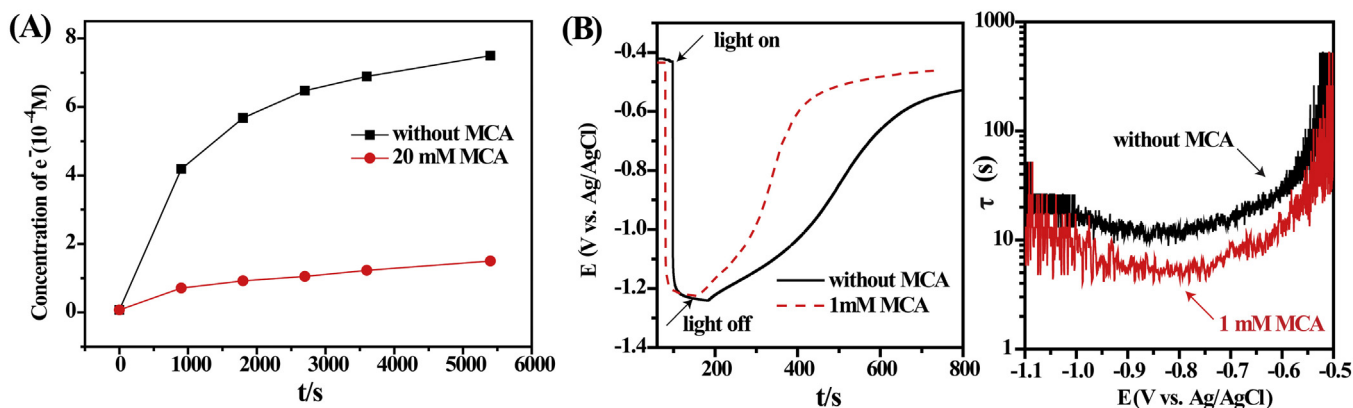
Fig. 2. (A) Electron concentration of TiO_2 suspension (20 g/L) in the presence and absence of 20 mM MCA under irradiation. (B) Open circuit potential profile of the TiO_2 electrode in the presence and absence of 1 mM MCA (left) and the corresponding electron lifetime (right) calculated using Eq. (1).
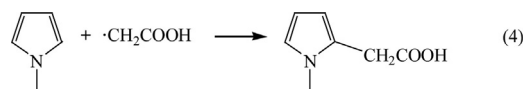
of 5 mM MCA (Fig. 3D and E). A plot of the absorbance at 2000 cm^{-1} against time (Fig. 3F) demonstrated that the electron accumulation was barely affected by MCA. The in situ ATR-MIR results agree with the OCP decay profiles, revealing that conduction band and shallow trapped electrons are less active in reductive activation of surface-attached C—Cl bond. The fact that rutile TiO_2 is active towards photocatalytic MCA reduction is consistent with the aforementioned argument, since the accumulated electrons in rutile are dominated by localized states and lack free carrier property (no MIR feature was reported for the rutile TiO_2) [32].

Although the difference between free and trapped electrons has been established in the photoreduction of triiodide and organic functional groups (e.g., aldehyde vs. nitro groups) using electrochemical measurements, only a few studies have advanced in visualizing their participation in interfacial electron transfer [29]. Using transient MIR absorption measurements, Yamakata et al. revealed a rapid reaction between molecular oxygen with the conduction band electron but not with localized Ti^{III} in rutile [33]. Free electrons are often found to be more active and show significantly higher electron transfer rate constant, e.g., the recombination of TiO_2 electrons with triiodide (in a dye-sensitized solar cell) or with a surface-trapped hole [15,18,28,29]. Herein, the bidentate coordination of MCA to the surface Ti_{5c} site (Fig. S5) [34,35] may contribute to the observed activity of localized Ti^{III} states. It has been suggested that formation of these localized states in the bandgap is more favorable at material surface or first layer subsurface [36–38]. Concerning these, the electron transfer activation of C-Cl could be promoted via an enhanced electronic coupling between Ti^{III} and the surface attached C-Cl σ* orbital. The localized Ti^{III} in lattice bulk can approach to surface by rapid site to site hopping [36,39] to trigger the surface reaction. Alternatively, two surface Ti^{3+} sites work in concert, promoting the overall two-electron transfer process [19]. The latter could also contribute to the high selectivity of hydrogenation, in competition with radical coupling process yielding other products. However, it is not conclusive that the surface coordination and/or location of Ti^{III} are the dominant reasons for our observations. We are carrying ongoing studies to reveal origins of distinct activities of various electronic states in reduced TiO_2.

It is also worth to note that platinized TiO_2 (0.5 wt%) was not efficient for reductive conversion of MCA. As show in Fig. S6, only 15% of MCA was reduced, instead, continuous evolution of hydrogen was observed. Under this condition, the photogenerated electron was transferred to Pt for the subsequent reaction [40]. The suppressed conversion of MCA on Pt-TiO_2 supports a critical role of Ti^{III} states of TiO_2 in electron transfer activation of C—Cl bond.

The photocatalytic reduction intermediates $^•CH_2COOH$ was identified by its characteristic addition to N-methylpyrrole, pro-

ducing 1-methylpyrrole-2-acetic acid (Eqs. (3) and (4), Supporting contents, Fig. S7) [41,42]. This result indicates an initial dissociative electron transfer to break C-Cl, releasing Cl$^-$. A mechanism of concerted DET, i.e., the electron transfer and C-X bond dissociation occur in a single kinetic step, was suggested for aliphatic halide by electrochemical studies and DFT calculations. By avoiding the high-energy anion radical intermediates, concerted DET is more thermodynamically favored in comparing to stepwise DET [43–46]. However, the standard reduction potential (SRP) for this step is not experimentally accessible, and the observed irreversible peak potentials for most organic halides are considerably more negative than SRP [47]. For ethyl chloroacetate, the ethyl ester of MCA, the observed reductive peak potential (E_p) was between −1.5 and −2.08 V vs. SCE, whereas the calculated SRP for RX/R,X$^-$ (via DET) was −0.83 V vs. SCE [44,47]. The actual SRP of MCA could lie below the TiO_2 conduction band (-1.12 V in methanol) [11,48], rendering an energetically favored electron transfer to break the C—Cl bond.

$$TiO_2(e^-) + ClCH_2COOH \rightarrow {}^•CH_2COOH + Cl^- \tag{3}$$

$$\text{(4)}$$

We further explored the photoactivity of TiO_2 towards 3-chloropropionic acid (1b), 4-chlorobutyric acid (1c), and three monobromo analogues (2a–2c) (Table 1). According to the semiclassical theory, the electron transfer rate constant between donor and the surface coordinated acceptor can be described by Eq. (5), where H_{AB} is the electronic coupling matrix factor, λ is the reorganization energy and $\Delta G^{0'}$ is the standard free energy change [49]. The extended chain length increases the interfacial electron transfer distance, thus modifying the electronic coupling matrix element, as well as the reorganization energy [15,49,50]. Moreover, as the number of intervening carbons between the electron withdrawing carboxylic group and C-X increases, a negative shift in SRP is expected because the "bond-weakening" effect of —COOH [46] fades with distance. The consecutive changes in redox potential and the electron transfer distance allow analysis of the key factors that govern the C-X bond activation at the interface.

$$k_{D-A} = \frac{2\pi}{\hbar} \frac{1}{\sqrt{4\pi\lambda k_B T}} |H_{AB}|^2 \exp\left(-\frac{(\Delta G^{0'} + \lambda)^2}{4\lambda k_B T}\right) \tag{5}$$

The variation of reduction potential was estimated by cyclic voltammetry on a glassy carbon electrode in acetonitrile. No reductive peaks were resolved for the halogenated carboxylic acids; therefore, experiments were performed for the ethyl ester form of the selected compounds (1a'–1c' and 2a'–2c', Table 1 and Fig. S8).
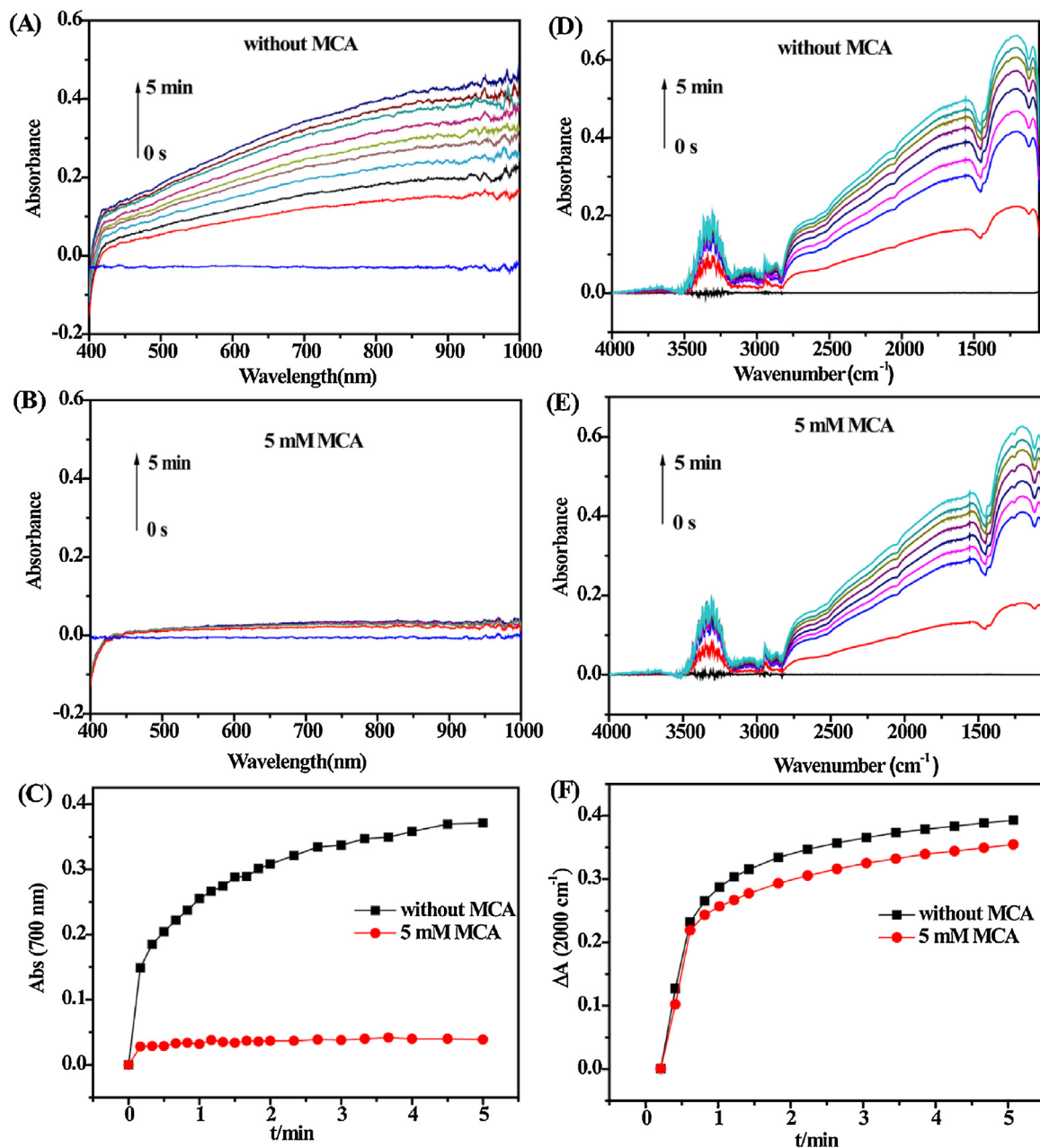
Fig. 3. UV–vis spectra of TiO$_2$ methanol suspension in the absence (A) and presence (B) of 5 mM MCA monitored during irradiation with a 3 W 365 nm LED light source. (C) Changes in absorption at 700 nm. Time-resolved ATR-MIR spectra during UV-irradiation of the TiO$_2$ film on a ZnSe crystal immersed in (D) methanol and in (E) 5 mM MCA methanol solution. (F) Changes of the IR absorbance at 2000 cm^{-1}.

Table 1
Photocatalytic reduction rates of halocarboxylic acids[a] and the reductive potentials of ethyl esters of the halogenated acids.

	RX[b]	Initial rate, (M h^{-1})		RX	E$_p$(vs. Ag/AgCl)[c]
1a	ClCH$_2$COOH	0.28	1a'	ClCH$_2$COOEt	−2.22
1b	Cl(CH$_2$)$_2$COOH	4.63 × 10^{-3}	1b'	Cl(CH$_2$)$_2$COOEt	−2.45
1c	Cl(CH$_2$)$_3$COOH	nd	1c'	Cl(CH$_2$)$_3$COOEt	<−3.0
2a	BrCH$_2$COOH	2.14	2a'	BrCH$_2$COOEt	−1.77
2b	Br(CH$_2$)$_2$COOH	7.41 × 10^{-3}	2b'	Br(CH$_2$)$_2$COOEt	−2.36
2c	Br(CH$_2$)$_3$COOH	nd	2c'	Br(CH$_2$)$_3$COOEt	<−3.0

[a] TiO$_2$: 0.5 g/L, solvent: CH$_3$OH, light Source: 300 W lamp light with 360 nm cutoff filter, temperature: 303 K, atmosphere: Ar.

[b] 1 mM concentration.

[c] Reductive peak potential obtained in acetonitrile with 1 mM ethyl esters of the halogenated acids, electrolyte was 0.1 M n-Bu$_4$NBF$_4$, the working electrode was glassy carbon.

As expected, E$_p$ of bromo-substitutes is less negative than those of chlorinated analogues, and E$_p$ negatively shifts from acetic to butyric esters (Table 1). Again, the SRP values of these compounds

are expected be more positive than the E$_p$ obtained in CV; however, the trend of SRP for 1a-1c and 2a-2c should remain the same. The molecular radii of 1a-1c are estimated to be 0.232, 0.296 and
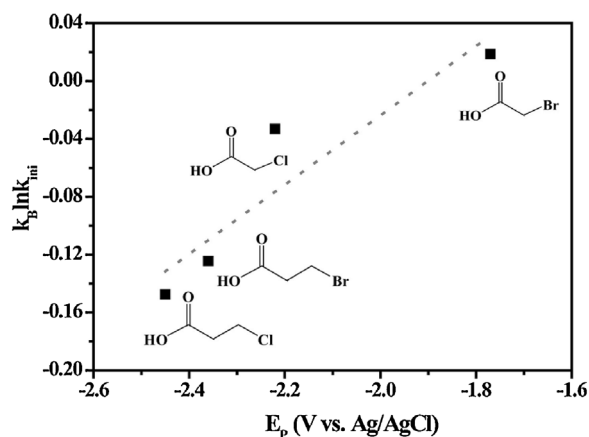
Fig. 4. Plot of $k_B T \ln k_{ini}$ vs. E_p observed for ethyl esters of the listed acid. The dashed line guides the linear fitting of the plot.

0.358 nm in the optimized configuration by DFT calculation (Supporting contents, Fig. S9). According to Eq. (S1), the outer-sphere reorganization energies of electron transfer at semiconductor-molecular interfaces for 1a to 1c are calculated as 1.20 eV, 0.94 eV and 0.76 eV [15,51].

As shown in Fig. S10, the pseudo-first order rate constant of monobromoacetic acid (2a) debromination is 1.4×10^{-3} s^{-1}, one order of magnitude higher than that of MCA. For 3-bromopropionic acid (2b), a 24 h irradiation caused 55% debromination however the selectivity of propionic acid dropped to 20%; less than 20% conversion was observed for 3-chloropropionic acid (1b), 4-chlorobutyric acid (1c) and 4-bromobutyric acid (2c) under the same conditions. The initial rates observed in the photocatalytic reduction decreased as follows: 2a > 1a (MCA) > 2b > 1b > > 2c, 1c (Table 1 and Fig. 4). Electron pre-stored on TiO$_2$ also show decreased activity towards halogenated propionic and butyric acids (Table S1). Although the actual driving force is not experimentally accessible, the plot of $k_B T \ln k_{ini}$ (k_{ini} is the initial rate) against the irreversible E_p for the ethyl ester analogues (Fig. 4) reveals that the electron transfer lies in the Marcus normal region, i.e., $\Delta G^{0\prime} < \lambda$ [49], and the decrease in the electron transfer driving force is responsible for the low activities of TiO$_2$ towards halogenated propionic and butyric acids. The precise contributions of H_{AB} and reorganization energy are not discussed here considering the large uncertainties in the actual SRP of the carboxylic acids and the rate constant of the elemental DET step (not the apparent photocatalytic dehalogenation rate).

4. Conclusions

In summary, the reductive dechlorination of MCA to HOAC and Cl$^-$ was realized with high selectivity on TiO$_2$ under UV irradiation with alcohol as the electron donor. The reaction was initiated by the rate-determining concerted dissociative electron transfer to break the C-Cl bond. In situ UV-vis-NIR and MIR measurements revealed that the localized Ti^{III} states were active towards MCA reduction. In contrast, conduction band and shallow trapped electrons has minor contribution to this process. Decreased activities were observed in the photoreduction of halogenated aliphatic acids with a longer chain length (propionic or butyric acids) due to the decrease in the electron transfer driving force. This work and our earlier studies on aromatic halides imply diverse electron transfer pathways that are collectively governed by the chemical nature of the accumulated electrons, the surface-substrate interactions and the free energy change in the elemental step. An exploration of the metal oxide semiconductor catalyzed activation of carbon

halogen bonds would be valuable for environmental remediation or radical-involved coupling reactions.

Appendix A. Supplementary data

Supplementary data associated with this article can be found, in the online version, at http://dx.doi.org/10.1016/j.apcatb.2017.07.056.

References

[1] M. Elsner, T.B. Hofstetter, Current perspectives on the mechanisms of chlorohydrocarbon degradation in subsurface environments: insight from kinetics, product formation, probe molecules, and isotope fractionation, in: P.G. Tratnyek, T.J. Grundl, S.B. Haderlein (Eds.), Aquatic Redox Chemistry, American Chemical Society, Washington, DC, 2011, pp. 407–439.
[2] R.M. Hozalski, L. Zhang, W.A. Arnold, Environ. Sci. Technol. 35 (2001) 2258–2263.
[3] L. Zhang, W.A. Arnold, R.M. Hozalski, Environ. Sci. Technol. 38 (2004) 6881–6889.
[4] X. Wang, P. Ning, H. Liu, J. Ma, Appl. Catal. B: Environ. 94 (2010) 55–63.
[5] J. Zhou, Y. Han, W. Wang, Z. Xu, H. Wan, D. Yin, S. Zheng, D. Zhu, Appl. Catal. B: Environ. 134 (2013) 222–230.
[6] Y.H. Xu, H. Zhang, C.P. Chu, C.A. Ma, J. Electroanal. Chem. 664 (2012) 39–45.
[7] M.D. Esclapez, M.I. Díez-García, V. Sáez, I. Tudela, J.M. Pérez, J. González-García, P. Bonete, Electrochem. Acta 56 (2011) 8138–8146.
[8] A. Li, X. Zhao, Y. Hou, H. Liu, L. Wu, J. Qu, Appl. Catal. B: Environ. 111 (2012) 628–635.
[9] R. Mao, N. Li, H. Lan, X. Zhao, H. Liu, J. Qu, M. Sun, Environ. Sci. Technol. 50 (2016) 3829–3837.
[10] H. Czili, A. Horváth, Appl. Catal. B: Environ. 89 (2009) 342–348.
[11] C. Schnabel, M. Wörner, B. González, I. del Olmo, A.M. Braun, Electrochem. Acta 47 (2001) 719–727.
[12] X. Li, J. Ma, G. Liu, J. Fang, S. Yue, Y. Guan, L. Chen, X. Liu, Environ. Sci. Technol. 46 (2012) 7342–7349.
[13] R. Fliount, O. Makogon, D.M. Guldi, K.D. Asmus, J. Chem. Soc. Perkin Trans. 2 (1997) 1535–1546.
[14] C. Kerzig, M. Goez, Chem. Sci. 7 (2016) 3862–3868.
[15] S. Kohtani, Y. Kamoi, E. Yoshioka, H. Miyabe, Catal. Sci. Technol. 4 (2014) 1084–1091.
[16] S. Kohtani, E. Yoshioka, K. Saito, A. Kudo, H. Miyabe, J. Phys. Chem. C 116 (2012) 17705–17713.
[17] K. Imamura, K. Hashimoto, H. Kominami, Chem. Commun. 48 (2012) 4356–4358.
[18] A. Molinari, A. Maldotti, R. Amadelli, J. Chem. Eur. 20 (2014) 7759–7765.
[19] Y. Li, H. Ji, C. Chen, W. Ma, J. Zhao, Angew. Chem. Int. Ed. 125 (2013) 12868–12872.
[20] Y. Shiraishi, H. Hirakawa, Y. Togawa, T. Hirai, ACS Catal. 4 (2014) 1642–1649.
[21] C. Liu, A.Y. Zhang, D.N. Pei, H.Q. Yu, Environ. Sci. Technol. 50 (2016) 5234–5242.
[22] W. Chang, C. Sun, X. Pang, H. Sheng, Y. Li, H. Ji, W. Song, C. Chen, W. Ma, J. Zhao, Angew. Chem. Int. Ed. 54 (2015) 2052–2056.
[23] C. Sun, D. Zhao, C. Chen, W. Ma, J. Zhao, Environ. Sci. Technol. 43 (2008) 157–162.
[24] W. Choi, M.R. Hoffmann, Environ. Sci. Technol. 29 (1995) 1646–1654.
[25] S. Kim, W. Choi, J. Phys. Chem. B 106 (2002) 13311–13317.
[26] Y. Yan, W. Shi, Z. Yuan, S. He, D. Li, Q. Meng, H. Ji, C. Chen, W. Ma, J. Zhao, J. Am. Chem. Soc. 139 (2017) 2083–2089.
[27] B.H. Meekins, P.V. Kamat, ACS Nano 3 (2009) 3437–3446.
[28] D. Monllor-Satoca, R. Gómez, J. Phys. Chem. C 112 (2008) 139–147.
[29] J. Bisquert, A. Zaban, M. Greenshtein, I. Mora-Seró, J. Am. Chem. Soc. 126 (2004) 13550–13559.
[30] T. Berger, M. Sterrer, O. Diwald, E. Knözinger, D. Panayotov, T.L. Thompson, J.T. Yates, J. Phys. Chem. B 109 (2005) 6061–6068.
[31] D.A. Panayotov, S.P. Burrows, J.R. Morris, J. Phys. Chem. C 116 (2012) 4535–4544.
[32] T. Berger, J.A. Anta, V. Morales-Florez, Phys. Chem. Chem. Phys. 15 (2013) 13790–13795.
[33] A. Yamakata, J.J.M. Vequizo, H. Matsunaga, J. Phys. Chem. C 119 (2015) 24538–24545.
[34] A. Mattsson, L. Osterlund, J. Phys. Chem. C 114 (2010) 14121–14132.
[35] F.P. Rotzinger, J.M. Kesselman-Truttmann, S.J. Hug, V. Shklover, M. Grätzel, J. Phys. Chem. B 108 (2004) 5004–5017.

[36] M. Setvin, C. Franchini, X. Hao, M. Schmid, A. Janotti, M. Kaltak, C.G. Van de Walle, G. Kresse, U. Diebold, Phys. Rev. Lett. 113 (2014) 086402.
[37] J. Bisquert, A. Zaban, M. Greenshtein, I. Mora-Seró, J. Am. Chem. Soc. 126 (2004) 13550–13559.
[38] P.M. Kowalski, M.F. Camellone, N.N. Nair, B. Meyer, D. Marx, Phys. Rev. Lett. 105 (2010) 146405.
[39] C. Spreafico, J. VandeVondele, Phys. Chem. Chem. Phys. 16 (2014) 26144–26152.
[40] Z. Lian, W. Wang, G. Li, F. Tian, K.S. Schanze, H. Li, ACS Appl. Mater. Interfaces (2016).
[41] Z. Chami, M. Gareil, J. Pinson, J.M. Saveant, A. Thiebault, J. Org. Chem. 56 (1991) 586–595.
[42] I. Ghosh, T. Ghosh, J.I. Bardagi, B. König, Science 346 (2014) 725–728.
[43] C.P. Andrieux, A. Le Gorande, J.M. Saveant, J. Am. Chem. Soc. 114 (1992) 6892–6904.
[44] A.A. Isse, S. Gottardello, C. Durante, A. Gennaro, Phys. Chem. Chem. Phys. 10 (2008) 2409–2416.
[45] A.A. Isse, A. Gennaro, C.Y. Lin, J.L. Hodgson, M.L. Coote, T. Guliashvili, J. Am. Chem. Soc. 133 (2011) 6254–6264.
[46] S.V. Rosokha, E. Lukacs, J.T. Ritzert, A. Wasilewski, J. Phys. Chem. A 120 (2016) 1706–1715.
[47] A.A. Isse, C.Y. Lin, M.L. Coote, A. Gennaro, J. Phys. Chem. B 115 (2010) 678–684.
[48] G. Redmond, D. Fitzmaurice, J. Phys. Chem. 97 (1993) 1426–1430.
[49] R.A. Marcus, N. Sutin, Biochim. Biophys. Acta 811 (1985) 265–322.
[50] K. Hu, A.D. Blair, E.J. Piechota, P.A. Schauer, R.N. Sampaio, F.G. Parlane, G.J. Meyer, C.P. Berlinguette, Nat. Chem. 8 (2016) 853–859.
[51] J.W. Ondersma, T.W. Hamann, J. Am. Chem. Soc. 133 (2011) 8264–8271.